J. Appl. Comput. Mech., 6(4) (2020) 757-776
DOI: 10.22055/JACM.2019.30011.1677

ISSN: 2383-4536
jacm.scu.ac.ir

M&MoCS

Shahid Chamran University of Ahvaz

Journal of Applied and Computational Mechanics

Research Paper

Torsional Aeroelasticity of a Flexible VAWT Blade using a Combined Aerodynamic Method by Considering Post-stall and Local Reynolds Regime

Sh. Shams[1], A. Molaei[2], B. Mirzavand[3]

[1] Assistant Professor, Department of Aerospace Engineering, Faculty of New Sciences and Technologies, University of Tehran Tehran, 1439957131, Iran, Email: shahrokh.shams@ut.ac.ir

[2] Ph.D. Candidate. Department of Aerospace Engineering, Faculty of New Sciences and Technologies, University of Tehran Tehran, 1439957131, Iran, Email: ahad.moalei@ut.ac.ir

[3] Assistant Professor, Department of Aerospace Engineering, Faculty of New Sciences and Technologies, University of Tehran Tehran, 1439957131, Iran, Email: mirzavand@ut.ac.ir

Received June 27 2019; Revised August 28 2019; Accepted for publication September 29 2019.
Corresponding author: Sh. Shams (shahrokh.shams@ut.ac.ir)

Abstract. The present research investigates the torsional aeroelasticity of the blade of an H-type vertical axis wind turbine subject to stall and post–stall conditions in various Reynolds regimes, which is experienced by the blade in a full revolution. In order to simulate the aerodynamics, a new model based on a combination of the Double Multi Streamtubes (DMST) model and the nonlinear multi-criteria Cl-α equations, which is depended on the local Reynolds number of the flow, has been proposed. The results indicate that using of multi-criteria function dependent on the Reynolds number for the Cl-α curve has improved the prediction of the torsional behavior of the blade in azimuthal rotation of the blade compared to using single-criterion functions and linear aerodynamics. The blade's aeroelastic torsion has been studied for various TSR values.

Keywords: Vertical axis wind turbine, Aeroelastic torsion, DMST, Static stall, Post-stall, Reynolds.

1. Introduction

Given the present-day global consent on the necessity of preserving the environment, a universal endeavor has begun to replace fossil fuels with renewable energy sources. Hence, increasing attention is being paid to wind energy, and academic and industrial effort is being made to develop wind turbines and to increase their efficiency. The goal is to understand more accurately the behavior of wind turbines by conducting leading-edge research and to facilitate widespread and economical usage of wind turbines by improving their efficiency and reducing costs [1]. Wind turbines are commonly divided into Horizontal Axis Wind Turbines (HAWT) and Vertical Axis Wind Turbines (VAWT). VAWTs possess certain advantages such as lack of dependence on the wind direction, low maintenance costs, possibility of being used in urban environments, simple structural configuration and less fatigue loading [2]–[4]. For this reason, they have drawn attention in recent decades. Among different VAWTs, straight-bladed varieties have had considerable growth due to their simple blade design [5]. New researches [6] have shown that the efficiency of VAWTs can be further improved. Fig. 1 displays a straight-bladed VAWT. On the other hand, simultaneously increasing the dimensions and reducing the weight of wind turbines is of concern in modern wind turbine design [7] . This highlights the importance of

Published online: October 02 2019

recognizing and taking into account fluid-structure interaction phenomena and aeroelasticity issues in turbine design. Numerous researchers around the world either have conducted or are currently have involved in research on vertical axis turbines from this perspective. The following presents some works in this field.

Fig. 1. An H-type vertical axis turbine [6]

Before all, a brief discussion of the modelling techniques used in airfoil design and aerodynamic in VAWTs are presented. Due to the non-constant flow behavior, the blade's airfoil must be carefully selected since the torque produced by the blades depends on the lift and drag coefficients. Travis et al in 2012 [8] introduced and demonstrated a fully automated process for optimizing the airfoil cross-section of a vertical-axis wind turbine (VAWT) using CFD method to maximize the torque While implementing the constraints of conventional wind turbine design such as tip speed ratio, solidity, and blade profile. Battisti et al. in 2016 [9] compared the effect of the DU 06-W-200 and the NACA 0018 airfoils camber line on power and thrusts of a VAWT as a function of blade azimuthal position and TSR. They showed that DU 06-W-200 cambered airfoil increases rotor performance at starting TSRs at low rotor speed. However, limits the use of wind resource at low or medium speeds, which is typical in urban environments. Meana fernandez et al [10] in 2018 investigate Optimization of airfoil geometry for vertical-axis wind turbine using JavaFoil, a panel method software. They found that an increase on the airfoil thickness led to more significant lift production and a delay on the stall angle. In addition, they see that the addition of a small amount of camber to a symmetrical airfoil increases the lift and decreases the drag values with respect to the symmetrical one, but at the cost of a slight decrease in the stall angle. It was found that thickness values around 18 and 21% and camber values below 4% offer the best results. However, it should be noted that the construction of curved airfoils would be expensive. Paraschivoiu et al in 2018 [11] investigated advantages and the drawbacks of the use of symmetrical, cambered, and laminar airfoil for a typical Darrieus type VAWT. The NACA 0018, FX63-137, and SNLA 18/50 airfoils were selected for this study. The numerical tool used during this analysis (CARDAAV) is based on the improved DMST model.

There are generally three categories of aerodynamic models for vertical axis turbines: Momentum-based models, Vortex Theory-based models and cascade model [4]. The first two methods are frequently used. In addition to these, a variety of computational fluid dynamics (CFD) methods can also be used to perform aerodynamic calculations of wind turbines. Momentum-based models are based on mass and momentum Consistency. The momentum theory is the most important method for analyzing the aerodynamic characteristics of blade both for HAWT and VAWT [4]. Many efforts have been made to develop this concept over the years [5]. The first momentum-based model was developed by Templin in 1974 [12]. In this model (SST), it is assumed that the flow passes rotor inside a tube called Stream Tube, the rotor in this model is considered as Actuator Disk (Fig. 2). This idea has already been applied to HAWT. To Improve this model, Strickland [13] introduced Multi Streamtube model (MST). Based on this model the induced velocity can be varied at different positions of rotor. This method is known in HAWT as the Blade Element Momentum (BEM) method. Continuing to improve this approach, Paraschivoiu [14] developed Double Multi Streamtube model that two sets of tubes models the upstream half of the rotor and the downstream of the rotor. Efforts are still underway to develop and improve this model, and this study is one of them. Momentum theory-based models are very efficient in terms of computational speed.

Models based on vortex theory use the principle of Kelvin's theory in which the change in circulation over time should be zero (eq.1) [16]. The vortex method can be divided into two categories in terms of describing a blade as a single line of vortex or a mesh of multiple panels (Fig. 3). One of the advantages of this model is that it takes into account the nonlinear effects of the vortices more accurately, so the main benefit of this method is when the vortex interaction becomes greater, such as at high tip speed ratio or high stiffness ratio. These methods are computationally more costly but more accurate in predicting aerodynamic forces.

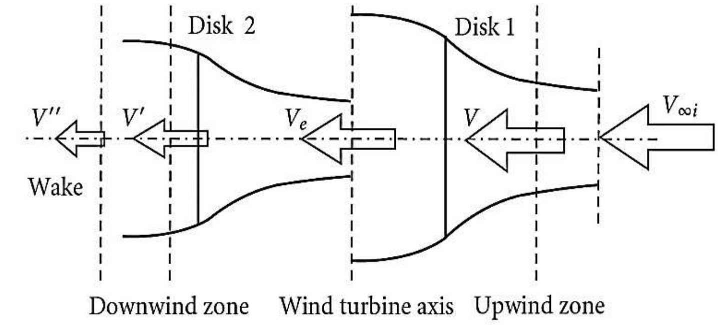

Fig. 2. A pair of actuator disks in tandem [15]

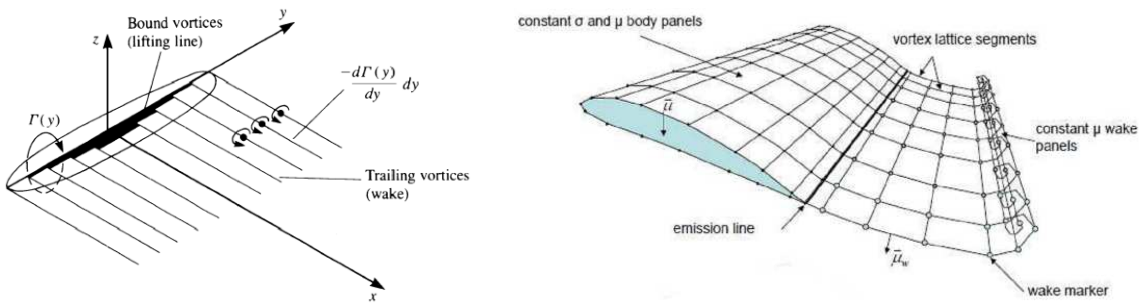

(a) (b)

Fig. 3. Discretization of a straight blade as: a) single line of vortex b) mesh of multiple panels [16]

$$\frac{D\Gamma}{Dt} = 0 \tag{1}$$

In 2012, Badiei et al. introduced a nonlinear aerodynamic pattern based on the Wagner function for modeling the effect of stall. They used line segments to represent the nonlinear part of the lift coefficient curve and were able to estimate this nonlinear part more accurately by increasing the number of the line segments [17]. In a research published in 2013, Lanzafame and Messina [18] investigated the effects of post-stall on improving BEM theory and the consideration of radial flow on the blade in a HAWT and, as a result, obtained analytical results for turbine efficiency that were close to experimental results. In 2013, Hameed and Afaq [19] carried out numerical and analytical studies on the loading of an H-shaped turbine blade and calculated the optimum airfoil thickness based by analyzing the stresses caused in the blade. In 2014, Brusca et al. [20] studied the impact of the aspect ratio of an H-shaped VAWT on its efficiency. They employed the MST model in the analysis and concluded that decreasing the aspect ratio of the turbine would improve its performance. In 2015, Tjiu et al. [21] presented a paper investigating different configurations of Darrieus vertical axis wind turbines. They also pointed out the obstacles preventing the large-scale production of each of these configurations. Various parameters including performance, components, and operational reliability have been evaluated in this paper. In addition, current advances and the development prospects of VAWTs have been presented. In 2015, Liu et al. studied the impact of blade flexibility in an H-shaped VAWT, concluding that a turbine with highly flexible blades has less power than one with solid blades [22]. In 2016, Brahimi, Saeed, and Paraschivoiu [23] investigated aerodynamic models for analyzing VAWTs. Their investigations concern details of the development procedure of various aerodynamic tools including the simulation of the flow between the blades, viscous flow, statistical wind, and stall dynamics effects. A comparison among the models indicates that the codes written based on the Double-Multiple Stream-Tube (DMST) model are more powerful in terms of simplicity, accuracy, and the ability to take into account secondary aerodynamic effects. In 2016, Shams et al. modeled a two-dimensional airfoil by considering third-degree nonlinearity for the aerodynamics and structural nonlinearity. The novel aeroelastic pattern they proposed eliminates the errors involved with the numerical simulation in addition to having higher accuracy in modeling the aeroelastic behavior of the airfoil after static stall [24]. Marten et al. used the Nonlinear Lifting Line Theory for a VAWT for the first time in 2017 and were able to present a complete model for its aerodynamic behavior [25]. Qing'an Li et al. [26] in 2017 investigated the stall phenomenon associated with unsteady flow around the airfoil surface of a straight-bladed vertical axis wind turbine with numerical and experimental methods. In 2018, Paraschivoiu et al. [11] examined the advantages and disadvantages of various types of symmetrical and asymmetrical airfoils in relation to the efficiency of a VAWT. They used the DMST theory in this research to compute the relative angle of attack and the relative flow velocity. In 2018, Zhao et al. [27] studied the power of a rotating airfoil in a VAWT by considering the DMST aerodynamic model. Their results showed that by placing the airfoil in the appropriate pitch function, the turbine power increases. In 2019, J. Lin et al [28] proposed a comprehensive fatigue and ultimate strength analysis framework for

VAWTs. Using this proposed model, they could predict critical locations of fatigue and ultimate strength failure of the blade. Wu Z. et al in 2019 [29] investigated the effects of lateral wind gusts on the aerodynamic performance of VAWTs. A synthetic approach coupling CFD simulations and the DMST method is utilized to calculate VAWT performance. In the latest study conducted in 2019 in this field, Shams and Esbati [30] derived the aeroelasticity equations of the rotating airfoil by considering unsteady Loewy aerodynamics and succeeded in delaying flutter velocity by applying PID control to the pitch angle.

2. Problem Statement and Assumptions

The confrontation between aerodynamic forces (lift and torque), external forces (centrifugal force), and elastic forces (torsional resistance) in the turbine blades leads to aeroelastic phenomena such as the aeroelastic torsion of the blade which, in turn, results in an increase in the angle of attack, finally resulting in torsional divergence. Due to the vertical rotation of the turbine axis in VAWTs, the angle of attack and the flow over the wing in vary considerably depending on the angular position of the turbine, unlike in airplanes or even HAWTs. Therefore, the existing linear and nonlinear equations cannot take into account all these conditions, and especially synthesized aerodynamics are required for analyzing a rotating blade. This issue is the focus of the present paper, and the impacts of various parameters including wind velocity, turbine angular velocity, blade position (azimuthal angle) on the static torsion of the turbine blade in stationary and rotating states will be studied by presenting a combined method. This method includes the nonlinearities resulting from static stall and post-stall under the effect of changes in the Reynolds regime of the flow along with the relative angle and the relative flow velocity resulting from a full rotation of the turbine and structural nonlinearities. The method presented here may be used for other structural computations such as blade bending, flutter dynamic instability, and the like.

A VAWT blade experiences completely different conditions while rotating around the axis. Thus, in order to locate the blade, a full rotation of the blade around the turbine axis will be divided into 8 regions such that Position 1 corresponds to an angle of zero and Position 2 corresponds to an angle of 45°, and the interval will be named Region 1. The rest of the regions are specified in the same manner (Fig. 4).

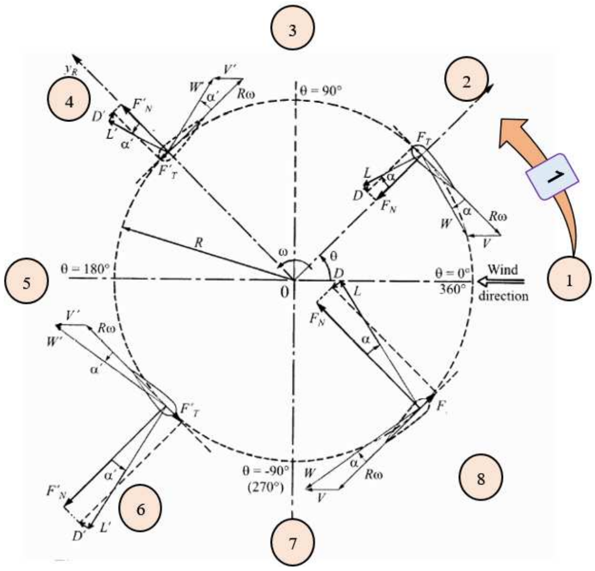

Fig. 4. Divisions of a full blade rotation and the corresponding flow vectors

The turbine blade is a typical section model with a torsional degree of freedom and a symmetrical NACA0018 airfoil. The torsion spring, which is in fact a model of the torsional resistance of the blade and its joints, has been considered as nonlinear and of degree 3. In addition, the airflow striking the turbine is uniform, incompressible, and subsonic.

3. Modeling and the Aerodynamics Governing Equations

The aerodynamic modeling involves three major challenges, namely calculating the local relative velocity and angle of attack, finding a model for applying the effects of Reynolds-dependent static stall and static post-stall, and merging the previous two results to compute the lift exerted on the blade at every position.

The theories used for calculating the relative angle of attack (α_D) and the relative flow velocity (W) in VAWTs include Single Stream-Tube (SST) [12] , Multiple Stream-Tube (MST) [31] , and Double-Multiple Stream-Tube (DMST) [32] among others. The DMST theory, which is the most evolved theory in this field [5], will be used in the present research. Reynolds-dependent multi-criteria polynomials will be employed to model stall effects. This process is displayed in Fig. 5. The mentioned points will be explained in the following.

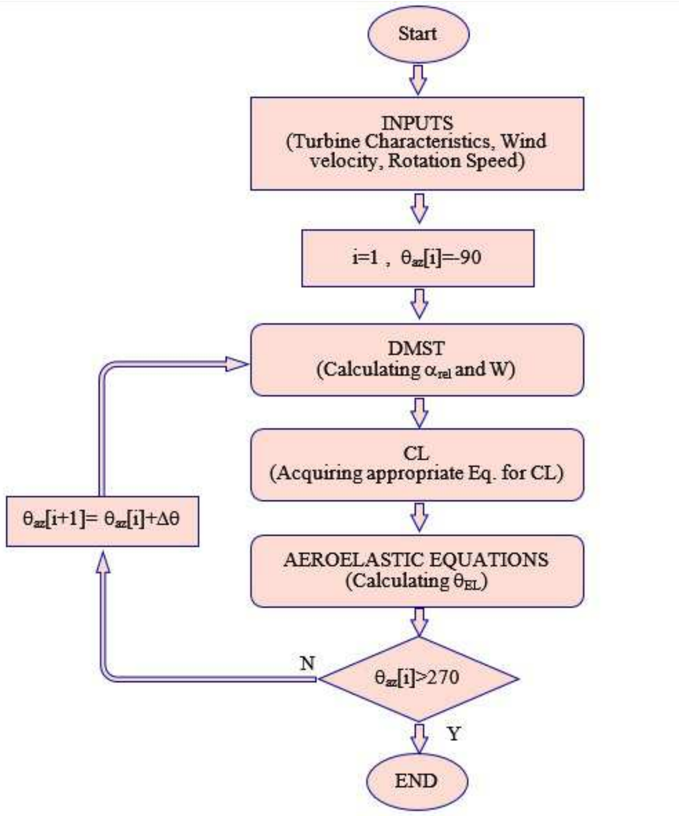

Fig. 5. Flowchart of the calculation process considered in the present research

3.1. Relative angle of attack and relative blade flow

Fig. **6** shows the modeling of a VAWT using the DMST method. In this model, the turbine is divided into upwind and downwind parts along with a number of tubes. This model takes into account the vortices created by the flow striking the front blade and the resulting reduction in velocity and wind energy on the rear blade. The airflow (V_∞) upwind of each tube strikes the front blades, loses energy and velocity (V), and reaches the downwind region where strikes the rear blades and exits the turbine (V'). It is assumed that the flows in different tubes are independent of each other.

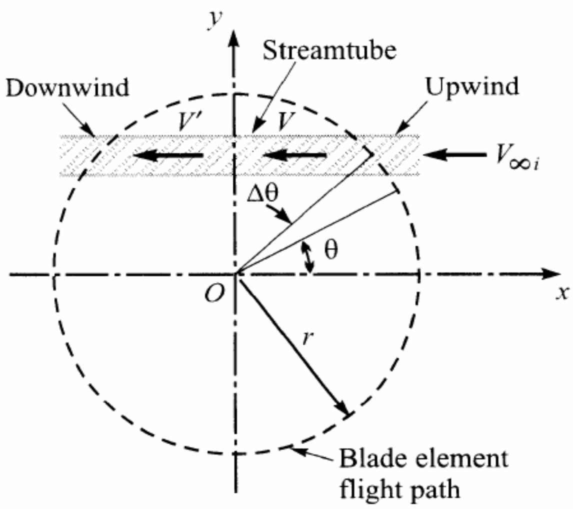

Fig. 6. Double-multiple stream-tube [15]

According to this theory, the relative velocity and the relative angle of attack are calculated separately at the upwind and downwind of the flow. In the upwind region, the relative flow velocity between the wind and the blade and the relative angle of attack of the blades are determined from the following equation:

$$W = V\sqrt{\left(\lambda - \sin\theta_{az}\right)^2 + \left(\cos\theta_{az}\right)^2} \tag{2}$$

$$\alpha_D = \sin^{-1}\left(\frac{\cos\theta_{az}}{\sqrt{(\lambda-\sin\theta_{az})^2+(\cos\theta_{az})^2}}\right) \tag{3}$$

$$v = uv_\infty \tag{4}$$

$$\lambda = R\Omega/V \tag{5}$$

In these relationships, V_∞ is the wind velocity at a location far from the turbine, ϑ_{az} is the angular position of the turbine blade (azimuthal angle), λ is the Tip Speed Ratio (TSR), and u is the induction factor in the upwind flow:

$$u(\theta) = \frac{KK_0}{(KK_0 + \int_{\theta_{az}-\frac{\Delta\theta_{az}}{2}}^{\theta_{az}+\frac{\Delta\theta_{az}}{2}} \left(\frac{W}{V}\right)^2 (C_N\cos\theta_{az} + C_T\sin\theta_{az}))} \tag{6}$$

$$k = \frac{8\pi R}{Nc} \tag{7}$$

$$K_0 = \sin\left(\theta_{az} + \frac{\Delta\theta_{az}}{2}\right) - \sin\left(\theta_{az} - \frac{\Delta\theta_{az}}{2}\right) \tag{8}$$

Here, C_N is the aerodynamic normal force coefficient, C_T is the aerodynamic tangent force coefficient, and R is the radius of the turbine.

$$C_N = C_L\,\mathrm{Cos}\,\alpha + C_D\,\mathrm{Sin}\,\alpha \tag{9}$$

$$C_T = C_L\,\mathrm{Sin}\,\alpha - C_D\,\mathrm{Cos}\,\alpha \tag{10}$$

C_L and C_D, respectively the lift and drag coefficients of the blade cross-section, are obtained using experimental data from NASA or Sandia National Laboratories, given known Reynolds number and angle of attack. The local Reynolds number of the blade is determined as follows:

$$\mathrm{Re}_b = Wc/v_\infty \tag{11}$$

ν_∞ denotes the kinematic viscosity of the flow. By defining the turbine Reynolds number as:

$$\mathrm{Re}_t = R\Omega c/v_\infty \tag{12}$$

We have:

$$\mathrm{Re}_b = \frac{\mathrm{Re}_t}{\lambda}\sqrt{(\lambda-\sin\theta_{az})^2+(\cos\theta_{az})^2} \tag{13}$$

To calculate u in each tube, an iteration procedure must be performed. Equations and a procedure similar to those for the upwind are used to calculate the relative angle of attack and the relative flow velocity in the downwind. The upwind values of a tube are used as the initial values for the iteration process in the downwind to take into account the effect of the upwind conditions on the downwind conditions in the iteration process.

3.2. Lift coefficient formulation

One may not directly utilize empirical data in order to calculate the value of blade torsion, and a relationship for the lift coefficient in terms of angle of attack is required. In linear aerodynamics, the lift coefficient is expressed as follows:

$$C_L = C_{L\alpha}\alpha \tag{14}$$

Where, $C_{L\alpha}$ is considered as constant for small angles of attack in linear aerodynamics. Expressed more simply, it is equal to $C_{L\alpha}=2\pi$ according to two-dimensional thin airfoil theory. The assumption of a small angle of attack in a VAWT is not correct due to the rotation of the blade relative to the free flow given the relative angle of attack. For instance, in a stationary turbine, the angle of attack can take values between -90° and +90°, depending on the blade position. The relative angle of attack decreases with the rotation of the turbine but may still have a large value. For a more accurate lift coefficient, the nonlinear effects of flow separation at large angles of attack must be considered in its calculation. Flow separation effects are modeled as dynamics separation and static separation. The nonlinear effects are considered as static separation in this analysis. Hence, it is necessary to estimate an equation for CL for all ranges of the angle of attack. Shams et al. [24] have shown that polynomial equations can provide a good estimation of the lift coefficient despite their simplicity.

The lift coefficient for a symmetrical airfoil in the 0-to-90° range and for various Reynolds numbers is plotted in Fig. 7. It is worth pointing out that with a change in the flow Reynolds number, the lift coefficient also changes. Therefore, the coefficients of the equations must be estimated according to the flow Reynolds number. As seen in the figure, the experimental lift coefficients are different up to and slightly after the stall point, and the results overlap at all Reynolds numbers with an increase in the angle of attack. For any given Reynolds number, the static stall and the post-stall lift coefficient can be well approximated using a third-degree polynomial and a second-degree polynomial, respectively. Since the lift coefficient does not change considerably with a change in the Reynolds number in the post-stall region, a second-degree equation suffices for all Reynolds numbers.

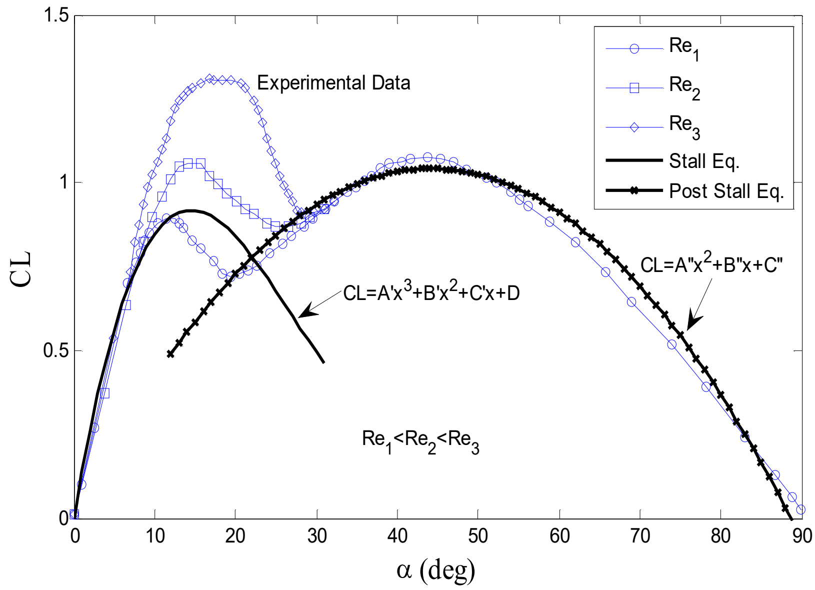

Fig. 7. Formulating stall and post-stall with polynomial equations

The angle of attack in a VAWT can range from -90° to +90°; therefore, three polynomials (one third-degree equation and two second-degree equations) are required to cover the whole range:

$$
\begin{aligned}
CL &= A''\alpha^2 + B''\alpha + C'' && for \quad -90 \le \alpha \le -\alpha_S \\
CL &= A'\alpha^3 + B'\alpha^2 + C'\alpha + D' && for \quad -\alpha_s < \alpha \le \alpha_s \\
CL &= -A''\alpha^2 + B''\alpha - C'' && for \quad -90 \le \alpha < -\alpha_s
\end{aligned}
\tag{15}
$$

The coefficients of the above polynomial are determined by substituting the boundary conditions from the experimental plot. For example, for a third-degree polynomial, the boundary condition coefficients are as follows:

- First boundary condition: The lift coefficient is equal to C_{L0} at a zero angle of attack.
- Second boundary condition: The slope of lift coefficient is equal to $C_{L\alpha 0}$ at a zero angle of attack.
- Third boundary condition: Coordinates of the point of maximum lift coefficient
- Fourth boundary condition: Zero slope of the lift curve at the point of maximum lift coefficient

By substituting the boundary conditions for a symmetrical airfoil, the third-degree equation is obtained as follows:

$$C_L = A'\alpha^3 + C'\alpha \tag{16}$$

It can be seen that parameter A' simulates the static stall and parameter C' is the slope of the CL-α graph at the zero point. The increase in the parameter A' and the creation of the static stall effect on the lift coefficient are seen in Fig. 8. By substituting A'=0, the linear lift coefficient is obtained, and by reducing A' (which is a negative number), the stall effects begin to appear. The appropriate function is obtained by superposing the graph onto that of empirical data for the desired airfoil and Reynolds number.

The coefficients of the equations for various Reynolds numbers are displayed in Table 1. In addition, the CL-α has been plotted in Fig. 9 for the linear form, equivalent polynomials, and experimental data for the NACA0018 airfoil at Re = 3.6e+5 using experimental data from reference [33].

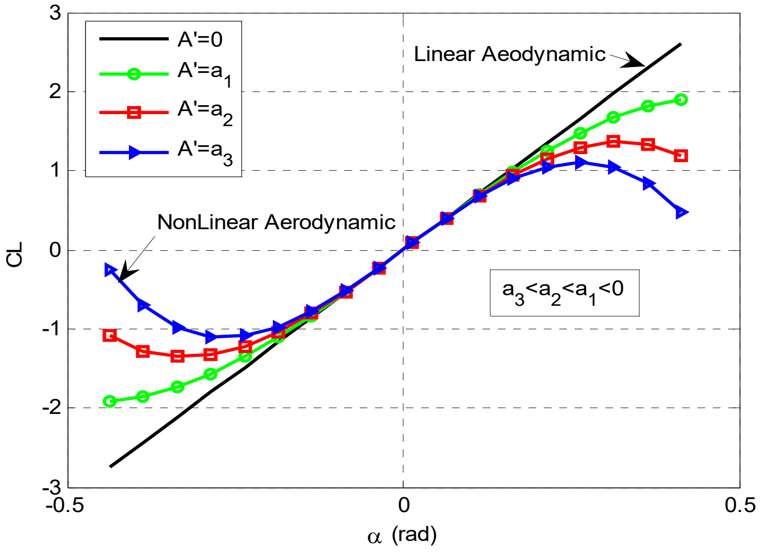

Fig. 8. The effect of coefficient A' (equivalent to static stall) on the lift coefficient

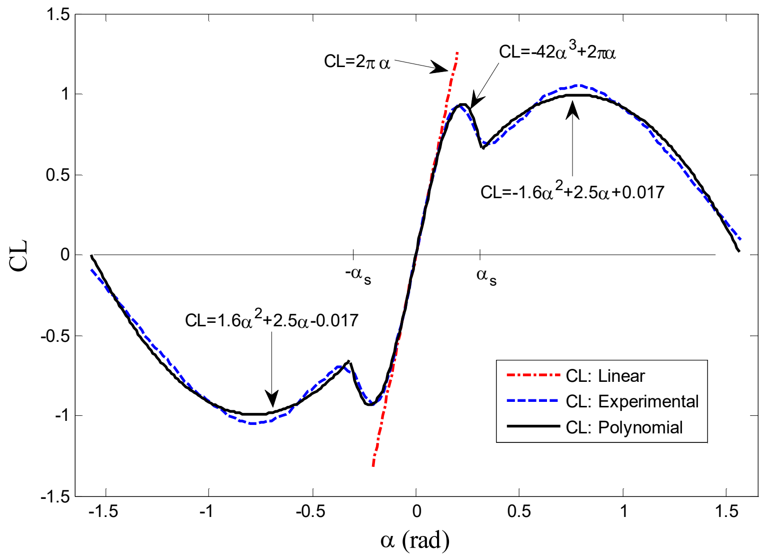

Fig. 9. CL-α for the linear state, experimental data, and equivalent polynomials for the NACA0018 airfoil and Re=3.6e+5

Table 1. Coefficients of polynomials equivalent to the lift coefficient of the NACA0018 airfoil

Reynolds	A'	C'	A''	B''	C''	α_s (rad)	Range (×10^5)
Re_1=160,000	-56.0	6.3	-1.6	2.5	0.017	0.27	<2.6
Re_2=360,000	-42.0	6.3	-1.6	2.5	0.017	0.32	2.6~4.3
Re_3=500,000	-40.6	6.4	-1.6	2.5	0.017	0.33	4.3~6.0
Re_4=700,000	-39.5	6.6	-1.6	2.5	0.017	0.34	6.0~8.5
Re_5=1000,000	-37.5	6.7	-1.6	2.5	0.017	0.36	8.5~20
Re_6=5,000,000	-24.0	6.8	-1.6	2.5	0.017	0.46	>20

The presence of airflow stall and the resulting nonlinearity of the lift coefficient cause the instability velocity and the aeroelastic torsion to be different from those for the linear lift coefficient. In this paper, the linear aerodynamic and the nonlinear aerodynamic states are compared.

4. Modeling the Aeroelasticity Equation of a Rotating Blade

This paper is concerned with the elastic torsion of the turbine blade; hence, one may assume each blade as a solid airfoil connected to a torsion spring by ignoring the bending flexibility of the blades. This torsion spring in fact models the torsional stiffness of the blade and the connections (Fig. 10). In this model, the torsion spring is at the elastic axis, the aerodynamic force and moment are exerted at the aerodynamic center, and the centrifugal force is exerted at the center of mass.

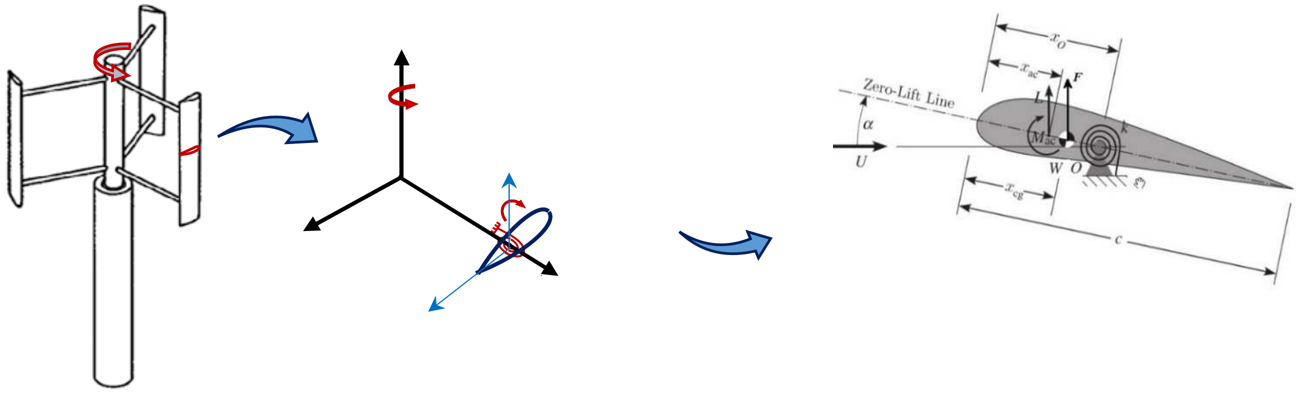

Fig. 10. Simplification of the rotating blade of a VAWT using the rotating airfoil (typical section) model

A balance of moments about the elastic center results in the following:

$$M_{ac} + L\left(x_0 - x_{ac}\right) + F\left(x_0 - x_{cg}\right) - M_s = 0 \tag{17}$$

$$M_{ac} = qScC_{Mac} \tag{18}$$

$$L = qSC_L \tag{19}$$

$$q = \frac{1}{2}\rho_\infty U_{rel}{}^2 \tag{20}$$

$$F = mR\Omega^2 \tag{21}$$

In this equation, Mac is the aerodynamic moment about the aerodynamic center and equals $C_{MAC}=0$ for symmetrical airfoils. L is the lift force, and F is the centrifugal force exerted on the blade due to turbine rotation, where R is the turbine radius and Ω is the angular velocity of the turbine. The important points in the aerodynamics of rotating airfoils relate to the terms α_{rel}, $U_{rel}=W$, and C_L, which were explained previously using the DMST theory and nonlinear aerodynamics. Finally, M_s is the resistant torsional moment of the blade, which can be modeled nonlinearly and with degree 3 according to the relationship below:

$$M_s = k_{\theta 1}\theta + k_{\theta 3}\theta^3 \tag{22}$$

By combining eq. 17 to eq. 22 and applying the equation of the nonlinear third degree lift coefficient, one obtains the following:

$$\frac{1}{2}\rho_\infty U_{rel}{}^2 S\left(A'\alpha^3 + C'\alpha\right)\left(x_0 - x_{ac}\right) + mR\Omega^2\left(x_0 - x_{cg}\right) - K_{\theta 1}\theta - K_{\theta 3}\theta^3 = 0 \tag{23}$$

Where, α is the total angle of attack, equal to the solid angle of attack plus the elastic torsion of the blade:

$$\alpha = \alpha_r + \theta \tag{24}$$

In which α_r is the solid angle of attack, and θ is the elastic angle of attack resulting from external forces. It must be noted that the solid angle of attack in a VAWT can be considered as the sum of two terms, namely the installation angle of the airfoil (α_m) and the relative angle of attack due to the rotation of the turbine (α_D obtained from the DMST theory):

$$\alpha_r = \alpha_m + \alpha_D \tag{25}$$

By substituting eq. 24 into eq. 23 and simplifying, one obtains the following:

$$\theta^3 + X\theta^2 + Y\theta + Z = 0 \tag{26}$$

where

$$X = \frac{qS\left(x_0 - x_{ac}\right)3\alpha_r A'}{qS\left(x_0 - x_{ac}\right)A' - K_{\theta 3}} \tag{27}$$

$$Y = \frac{qS\left(x_0 - x_{ac}\right)\left(3\alpha_r^{\ 2} + C'\right) - k_{\theta 1}}{qs\left(x_0 - x_{ac}\right)A' - k_{\theta 3}} \tag{28}$$

$$Z = \frac{qs\left(x_0 - x_{ac}\right)\left(A'\alpha_r^3 + C'\alpha_r\right) + mR\Omega^2\left(x_0 - x_{cg}\right)}{qS\left(x_0 - x_{ac}\right)A' - K_{\theta 3}} - \tag{29}$$

Furthermore, by substituting the second-degree lift equation into eq. 23, the following is obtained:

$$\theta^3 + X'\theta^2 + Y'\theta + Z' = 0 \tag{30}$$

where

$$X' = \frac{qS\left(x_0 - x_{ac}\right)A''}{-K_{\theta 3}} \tag{31}$$

$$Y' = \frac{qS(x_o - x_{ac})(2A''\alpha_r + B'') - K_{\theta 1}}{-K_{\theta 3}} \tag{32}$$

$$Z' = \frac{qS(x_o - x_{ac})(A''\alpha_r^2 + B''\alpha_r + C'') + mR\Omega^2(x_o - x_{cg})}{-K_{\theta 3}} \tag{33}$$

Equations 26 and 30 are standard third-degree polynomial functions and have classic solutions.

5. Validation

In order to ensure the validity of the model implemented in this research as MATLAB code for calculating the relative angle of attack of the rotating blade, the results obtained from the code have been compared to the values presented by Paraschivoiu, the inventor of this model [11]. The characteristics of the turbine and the required inputs are presented in Table 2. Fig. 11 presents the graph of changes in the relative angle of attack versus changes in the azimuthal angle of the turbine for X=1.52 and X=3.05 for the mentioned reference and the present work. The results are good and acceptable.

Table 2. Case Study characteristics

Parameter	Number of Blades	Rotor Height (H)	Rotor Diameter (D)	Airfoil Chord (c)	Blade Weight
Value	2	*5m*	2.5 m	0.1524 m	10 kg

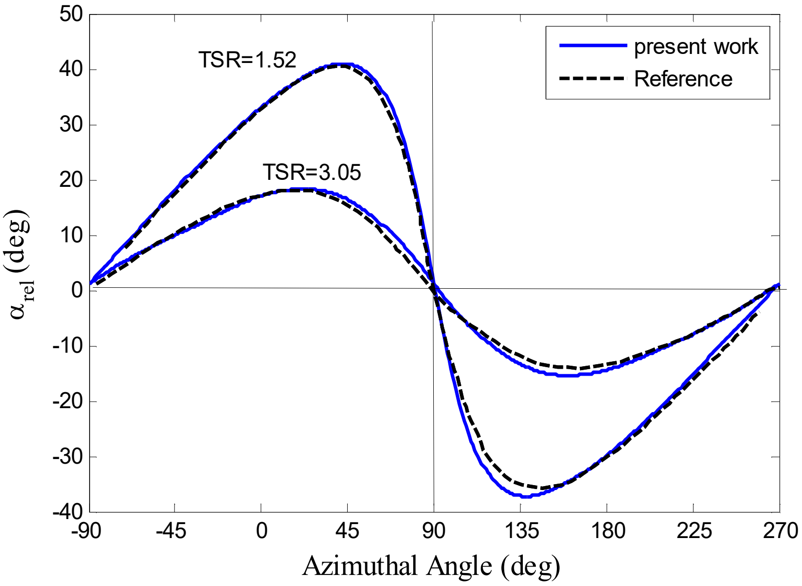

Fig. 11. Comparison between the results of the present work and Reference [11] for TSR=3.05 and TSR=1.52

Table 3. RMSE values of comparison angle of attack between present work and reference

	Upstream	Downstream	Total
X=1.52	0.63	1.51	1.17
X=3.05	0.81	0.95	0.88

The RMSE values for angle of attack discrepancy between current work and reference [11] in the upstream, downstream and total of turbine are given in Table 3. A part of the differences are due to rounding the experimental values of the CL and CD coefficients and the other part is related to the initial values, number of iterations and size of steps, etc. in the method. It is also evident that the differences in the downstream of the turbine are greater than the upstream of the turbine. This is due to the nature of the method in which upstream conditions (such as errors and inaccuracies) affect downstream conditions. The initial value of u (induction factor) at downstream of a tube equals to last u at the upstream of the same tube. This leads to that downstream differences (in addition to the above-mentioned items) to be affected by upstream.

In order to validate the MATLAB code written to compute the blade torsion, the divergence velocity for the item mentioned in Ref. [34] is determined and compared to the results of this reference. It is worth noting that the mentioned references have taken into account a linear lift coefficient; thus, the results here are based on the assumption of A'=0. The trends in the value of angle of attack versus an increase in the flow velocity are presented in Fig. 12. The graph tends to infinity at a velocity of U_D=104.2 (m/s). In Ref. [34], the divergence velocity is U_D=105.8 (m/s). Hence, a good agreement exists between the results.

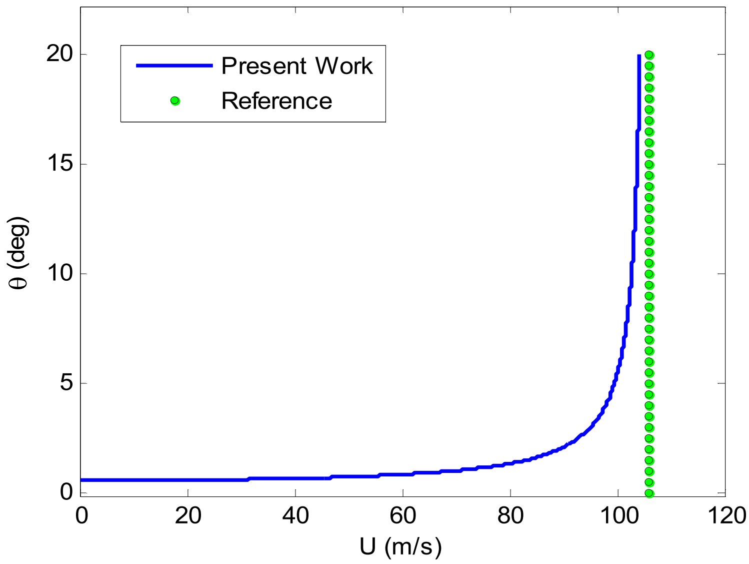

Fig. 12. Changes in linear aeroelastic torsion versus variations in the free flow velocity compared to Ref. [34]

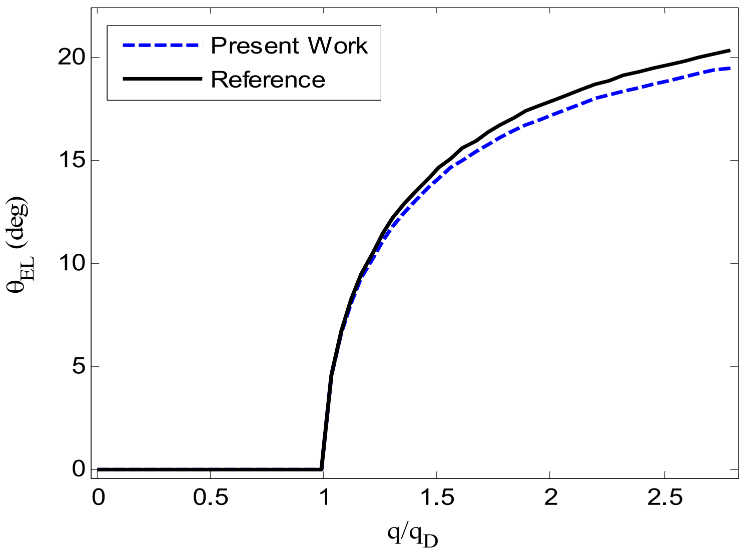

Fig 13. Comparison between the nonlinear aeroelastic torsion in this work and that of Ref. [35]

In addition, the graph presented in reference [35] has been considered in order to validate the presence of stall. This reference has plotted the graph of elastic torsion for a special case where the initial angle of attack is assumed zero. In the present research, the graph of the mentioned reference has been obtained by assuming α_r=0 (Fig 13). RMSE is calculated 0.49 and thus good agreement is observed. The horizontal axis of this graph has been made dimensionless in terms of the dynamic pressure of linear divergence (q_D) [35].

6. Results

6.1. Effect of a static stall on blade torsion

The impact of a static stall on the elastic torsion of the blade is plotted in Fig. 14. In this figure, the effect of static stall gradually increases, possibly due to a decrease in the Reynolds number or a change in the type of airfoil. It is observed that the linear and nonlinear aerodynamics coincide at small angles resulting from low flow velocities. With increasing flow velocity, the torsion angle intensely diverges at a specific velocity (the divergence velocity) in the linear state and tends to infinity. However, by considering the stall effects, the intensity of the elastic torsion decreases, and the elastic torsion will approach a specific value other than infinity. In other words, nonlinear aerodynamics predict the elastic torsion at higher flow velocities to be smaller than the value predicted by linear aerodynamics, due to the presence of stall and the reduction in the lift force.

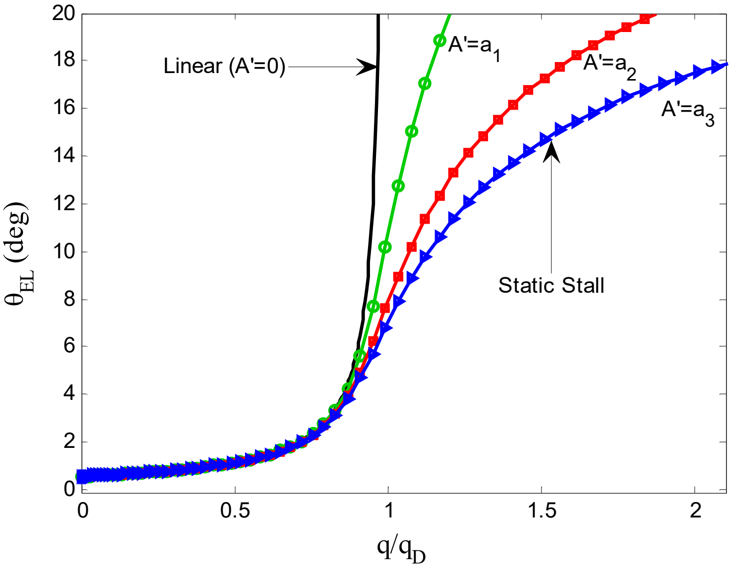

Fig. 14. Impact of a static stall on the elastic torsion of the airfoil

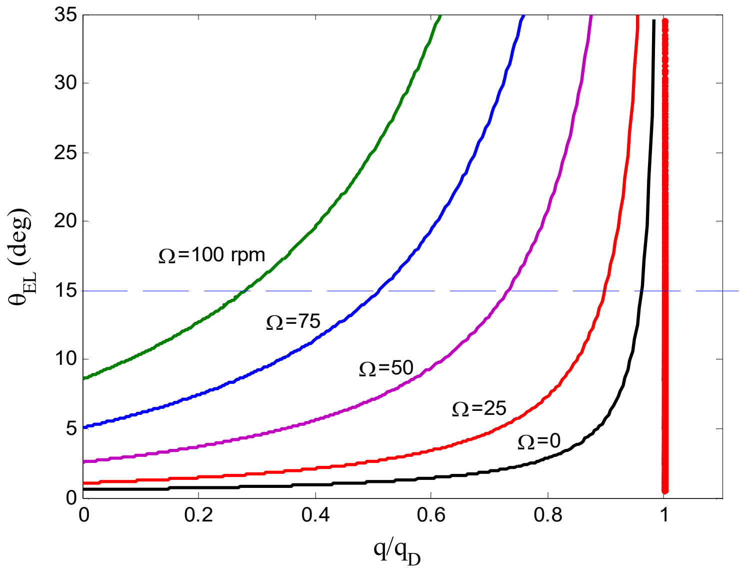

Fig. 15. Changes in the aeroelastic torsion angle versus changes in the angular velocity of the wind turbine with linear aerodynamics

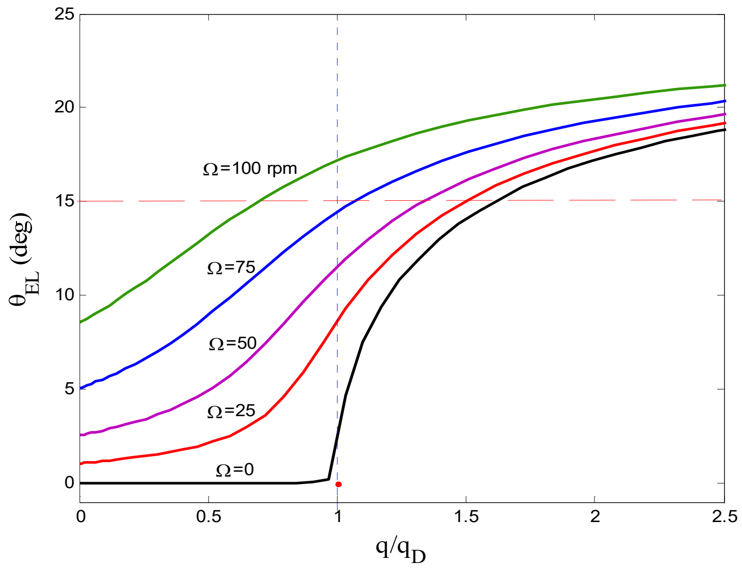

Fig. 16. Changes in the aeroelastic torsion angle versus changes in the angular velocity of the wind turbine with nonlinear aerodynamics

6.2. Effect of rotation on torsion

This part will study the effect of centrifugal force, which is affected by mass, turbine radius, and rotation velocity parameters. It should be noticed that the centrifugal force does not directly appear in the relationship relating to the divergence velocity with linear aerodynamics, but does appear in torsion relationship because it affects the torsion angle due to the impact of the solid angle of attack.

Fig. 15 and Fig. 16 display the variation in the elastic torsion angle with changes in the airfoil flow velocity for linear and nonlinear aerodynamics, respectively. The relative velocity is obtained by the vector addition of the wind velocity and the turbine angular velocity. These graphs have been plotted for a fixed turbine position where α_D=0 and with the assumption a constant Reynolds number of Re=3.6e+5. It must be noticed that in the divergence velocity, which is calculated using linear aerodynamics [34], the elastic torsion angle theoretically tends to infinity, but for nonlinear aerodynamics and nonlinear structure, the torsion angle tends to a specific value despite the sudden changes in its value at velocities corresponding to linear divergence. In other words, by taking into account the nonlinear effects of a stall and the nonlinear structural effects, the blade torsion will not exceed a certain limit. This torsion angle may as well be larger than the structure can bear and cause it to fail.

In Fig. 15 and Fig. 16, the black graph corresponds to zero angular velocity (stationary turbine); therefore, in this state, the horizontal axis represents the free wind velocity. With an increase in the turbine angular velocity, the centrifugal force causes an initial torsion angle in the blade and affects the trend of the increase in the elastic torsion angle. In the linear aerodynamics state, all the graphs tend to infinite torsion at the static divergence velocity. However, in the nonlinear state, they converge but do not tend to infinity.

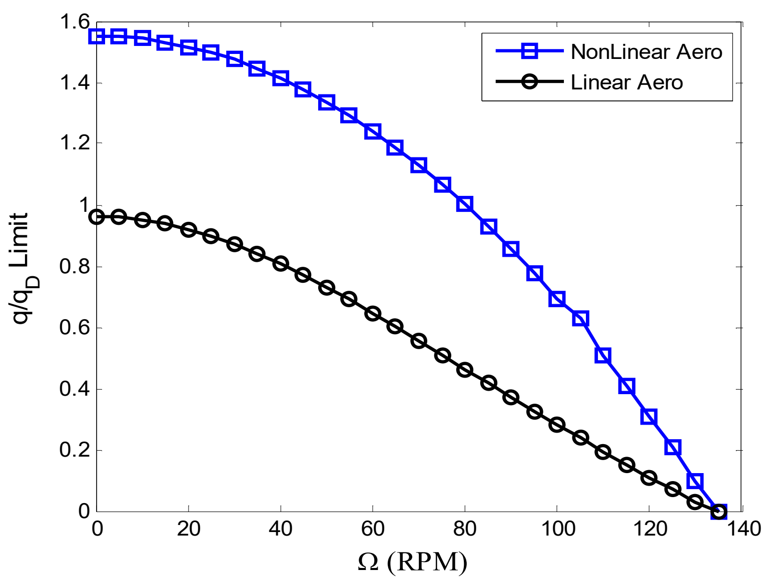

Fig. 17. Comparison between linear and nonlinear aerodynamics in predicting the permissible flow velocity

In real life, the blade is physically capable of tolerating a certain level of torsion. In other words, the turbine is allowed to operate in conditions where the blade torsion does not exceed the tolerable value. The flow velocity on top of the airfoil, which causes critical torsion, is called the permissible critical velocity. In addition, this critical torsion can be used as a basis for comparing different states and conditions. For example, if the tolerable torsion angle is assumed 15°, it is obvious based on Fig. 16 that with an increase in the angular velocity of the turbine, the allowable flow velocity decreases. For instance, according to the nonlinear analysis, a dynamic pressure ratio of q/q_D=1.24 (equivalent to a relative flow velocity of 58.7 m/s) is permissible for an angular velocity of 60 rpm, whereas it is q/qD=1.55 (equivalent to a relative flow velocity of 73.3 m/s) for a stationary turbine. The trend in the critical flow velocity versus turbine angular velocity for linear and nonlinear aerodynamics is plotted in Fig. 17. As mentioned previously, nonlinear aerodynamics predict a lower torsion and allow higher flow velocities due to taking into account stall effects and reducing the lift force at large angles.

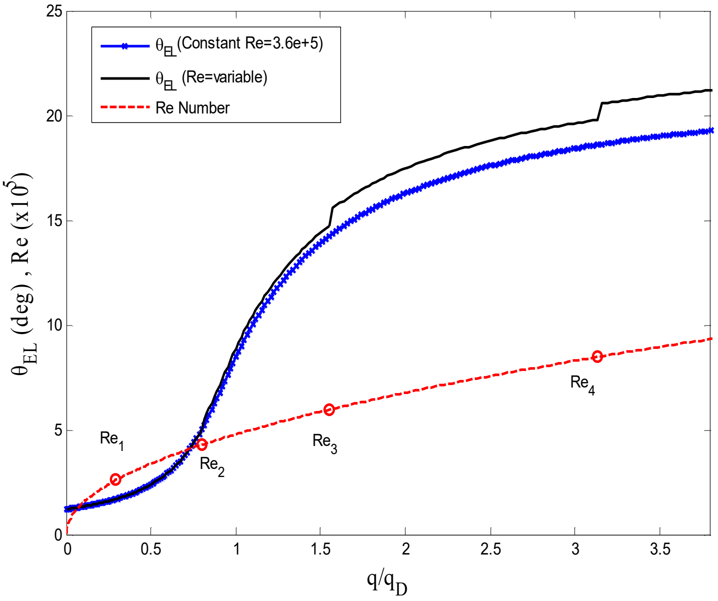

Fig. 18. Comparison of torsion for constant and variable Reynolds numbers

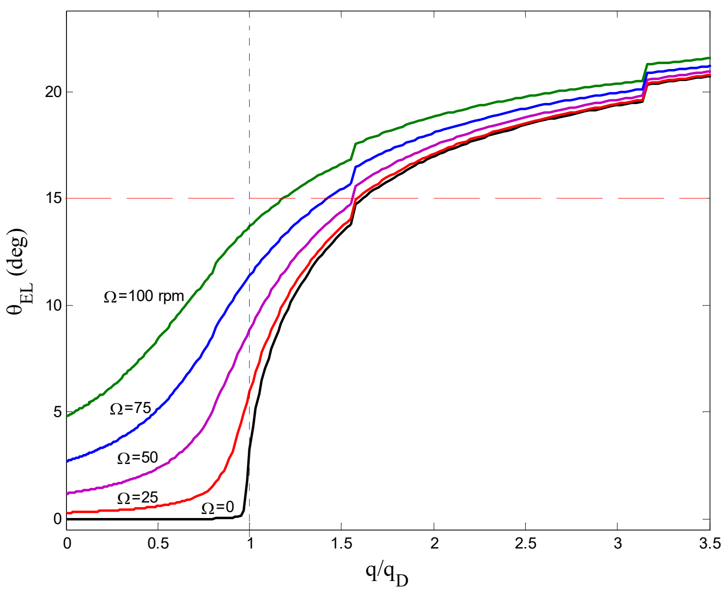

Fig. 19. Changes in the aeroelastic torsion angle versus changes in the angular velocity of the wind turbine with nonlinear aerodynamics and taking into account changes in the Reynolds number

6.2.1. Effect of the Reynolds number on the blade torsion

As mentioned before, changing the Reynolds number affects the CL-α curve such that the stall angle and the lift coefficient at the stall angle change. The effect of taking into account or ignoring the change in the CL-α curve due to the change in the Reynolds number during torsion is investigated here. The torsion graphs for constant and variable Reynolds numbers are plotted in the Fig. 18. The changes in the Re have also been added to this same graph. The coefficients related to the CL rule have changed according to Table 1 at the points specified on this curve. Consequently, the shift in coefficients has had jumps at these points on the torsion curve because the stall angle results in larger lift coefficients at high Reynolds numbers.

If the graphs of Fig. 16 are redrawn by considering the changes in the Reynolds number, the outcome will be the Fig. 19, which indicates results that are more accurate.

6.2.2. Comparing the results of linear, single-criterion nonlinear, and triple-criteria nonlinear aerodynamics

As mentioned before, due to the rotation of the VAWT, the blade experiences a wide range of different relative angles of attack and relative velocities during one full rotation. Obviously, the assumption of linear aerodynamics will be wrong if one aims to determine the blade torsion. Even the nonlinear aerodynamics of third-degree static stall will produce erroneous results at large angles of attack. As a result, a triple-criteria nonlinear aerodynamics is introduced in this paper to cover the curve at large angles of attack and produce rational results. Fig. 20 displays the elastic torsion of an airfoil governed by linear, single-criterion nonlinear, and triple-criteria nonlinear aerodynamics for TSR=3.05 and Ω=175 rpm in 360° of turbine azimuth. The small variation in Reynolds number has been ignored in these graphs. In addition, the relative angle of attack has been added to the same graphs for better demonstrating the occurrences. The first point is that, as predicted, the curve corresponding to linear aerodynamics is above nonlinear curves over the whole azimuth range. The curve and nonlinear curves approach each other at low angles of attack. However, the main issue has occurred in Regions 1 and 8. In these regions, the relative angle of attack has significantly increased and there is a wide discrepancy between linear and nonlinear aerodynamics, as clearly seen. Furthermore, it is important to notice the single-criterion and triple-criteria nonlinear curves. These two curves deviate from point a to point b. In this range, the angle of attack has exceeded 19° (which is common between the two curves), and the airfoil has entered the post-stall phase. The first CL rule, which is a third-degree polynomial, is completely erroneous in this region, and the task of computing the torsion angle has switched to the second curve; therefore, the desired correction is carried out. With the renewed reduction of the angle of attack below this value, the third-degree curve has taken over again and has performed the computations.

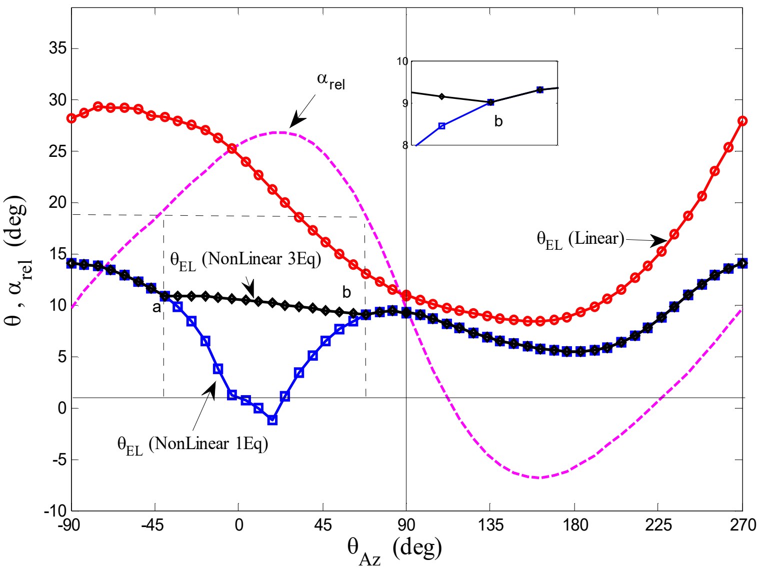

Fig. 20. Torsion under linear, single-criterion nonlinear, and triple-criteria nonlinear aerodynamics

6.3. Torsion exerted on the blades of a stationary turbine

Up to this point, the tools necessary for analyzing the structure of a VAWT (Reynolds-dependent multi-criteria equations combined with the DMST theory) were developed. Now, it is possible to analyze the structural behavior of the blades by combining the structural equations, considered here as a third-degree nonlinear torsion spring. In order to simplify the problem and eliminate the effect of rotation (and, therefore, the centrifugal force), a stationary turbine is considered first. For a stationary turbine in the parked position, changes in the elastic torsion of the blades in various positions are evaluated. The relative angle of attack is shown in Fig. 21. As expected, the angle of attack is zero at Positions 7 and 3 and 90° at Positions 1 and 5. This trend is dependent on wind velocity. Fig. 22 shows the relative velocity of the flow passing over the blade of the stationary turbine. As explained previously, the DMST theory can observe the effects on the downwind blades of fluctuations in flow caused by the flow striking the upwind blades. It is seen in this figure that with low-velocity winds, the flow velocity remains almost constant over the entire turbine; however, with an increase in wind velocity, the wind striking the upwind blades loses some energy and fluctuations appear in it, resulting in a reduced velocity at the downwind blades.

Fig. 23 displays the elastic torsion of the blade in the stationary turbine at various positions. Reynolds-dependent triple-criteria equations have been used in this graph. It is obvious that for a symmetric airfoil, no torsion occurs at Positions 3 and 7 due to the relative angle of attack being zero and at the upwind Position 1 and downwind Position 5 due to no lift force being created by the airfoil. As can be seen in the figure, Regions 2 and 7 are exposed to the largest torsion; therefore, they are the worst positions for the blade in terms of torsion. Assuming an angle of 15° for the critical torsion bearable by the blades, the allowable wind velocity for the considered stationary turbine is obtained to be 62 m/s.

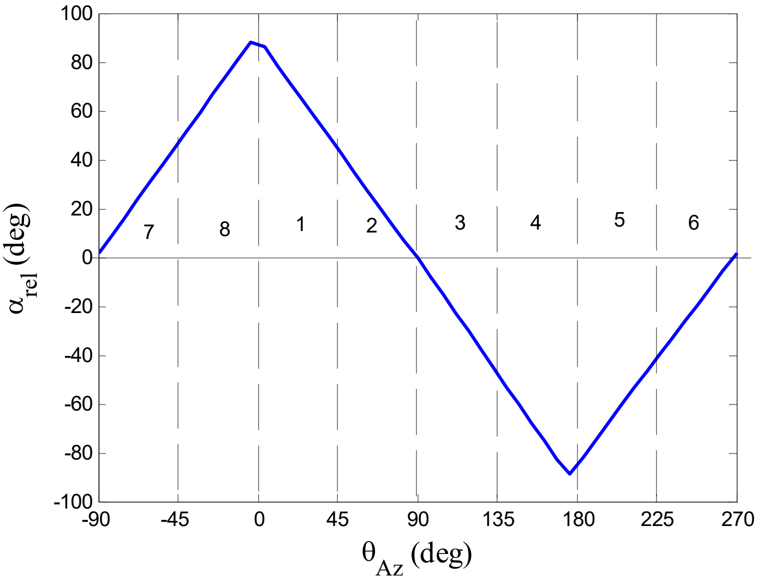

Fig. 21. Change in the angle of attack of the blade at azimuthal angles of the stationary turbine

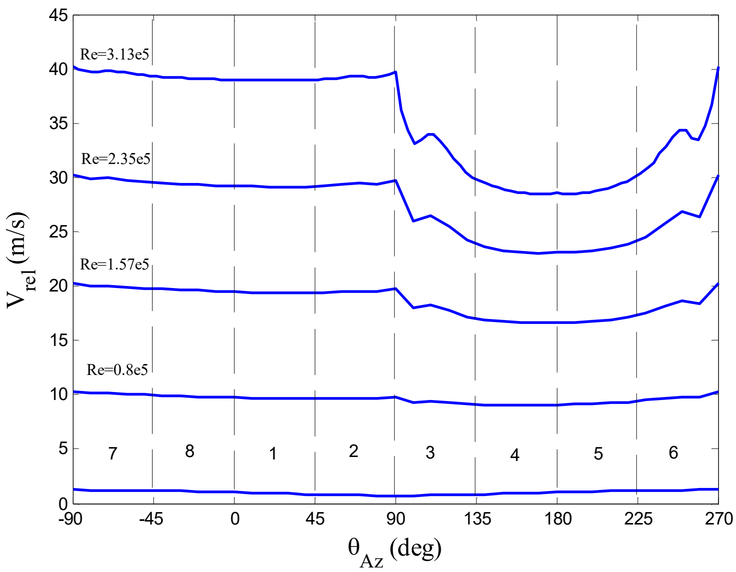

Fig. 22. Changes in the flow velocity on the blade at azimuthal angles of the stationary turbine

6.4. Blade torsion in rotating turbines

For 50 rpm, 100 rpm, angular velocities, the torsional behavior of the blade has been studied in one full rotation of the turbine at different TSR values. The results are shown in Fig. 24 to Fig. 28. The graph of Fig. 24 displays the relative angle of attack for TSR=1 to TSR=5. One must notice that this graph is independent of the angular velocity and dependent on TSR; therefore, it holds for all angular velocities. The graphs in Fig. 25 and Fig. 27 show the change in the local flow Reynolds number in one full rotation of the blade. The horizontal dashed lines represent the boundary between the low-Reynolds CL-α rule and the high-Reynolds one. It is seen that with an increase in TSR, the range of variation in the local Reynolds number is reduced. This affects the blade torsion shown in subsequent graphs. The torsional behavior of the blade in one full rotation at various TSR values are shown in Fig. 26 and Fig. 28. A comparison of these graphs indicates that the increase in the angular velocity due to (1) an increase in the centrifugal force, (2) an increase in the relative flow velocity and the resulting dynamic pressure exerted on the airfoil (q), and (3) an increase in the lift force due to a rise in the Reynolds number creates larger torsion. It also shows that an increase in TSR reduces the range of variation in torsion during one full rotation in both graphs. Hence, a lower angular velocity with a higher TSR is more desirable in terms of blade torsion. The largest torsion has occurred in Region 7 followed by Region 6. The transition from the beginning of Region 6 to the end of Region 7 will experience intense structural turbulence.

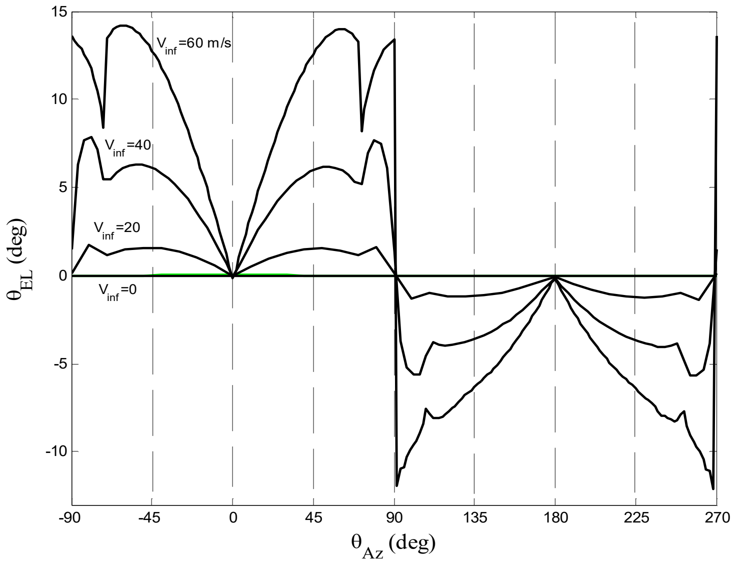

Fig. 23. Elastic torsion of the airfoil at azimuthal angles of the stationary turbine for various wind velocities

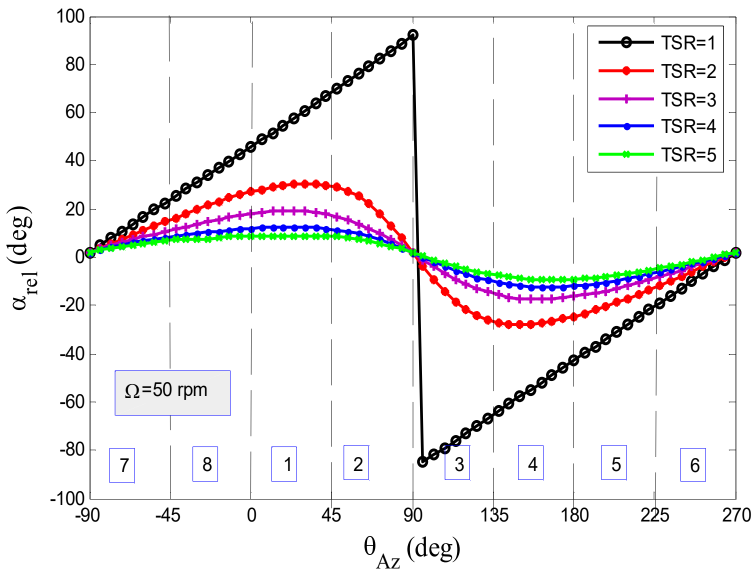

Fig. 24. Variation in the angle of attack versus the azimuth position at various TSR for Ω=50 rpm.

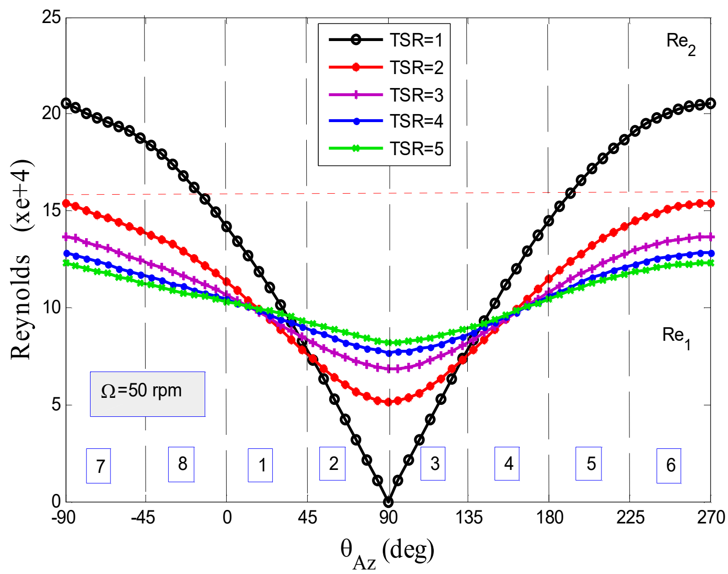

Fig. 25. Variation in the local Reynolds number for Ω=50 rpm at various TSR

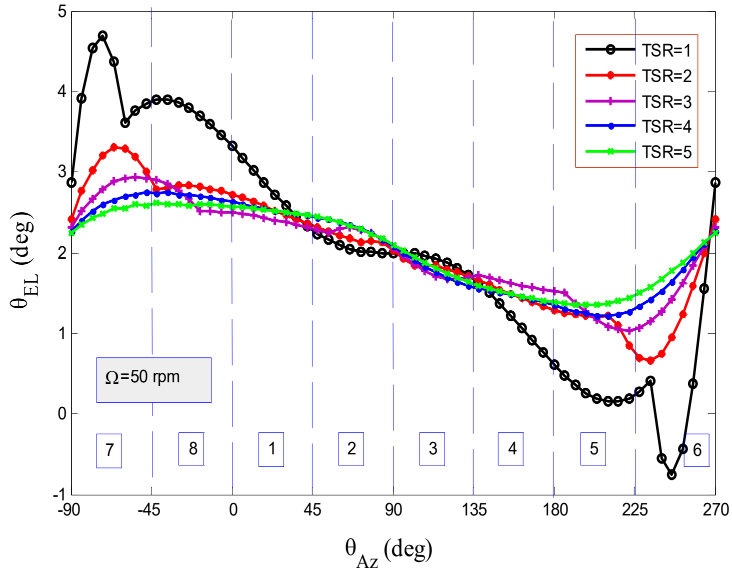

Fig. 26. Aeroelastic torsion of the blade at various azimuth angle for Ω=50 rpm

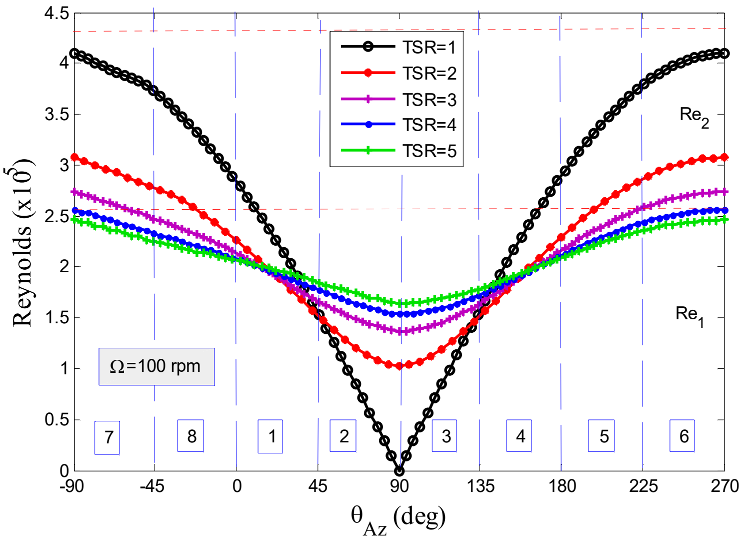

Fig. 27. Variation in the local Reynolds number for Ω=100 rpm at various TSR values

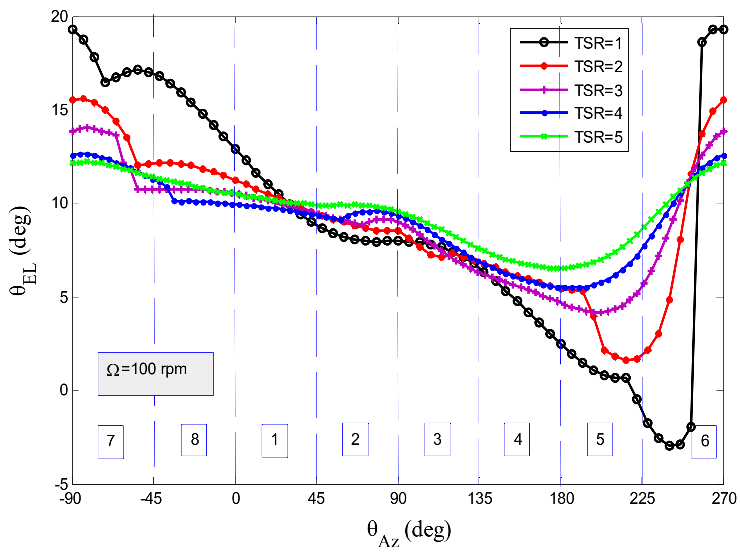

Fig. 28. Aeroelastic torsion of the blade at various azimuth values for Ω=100 rpm

7. Conclusion

In this research, a new method was presented for evaluating the aeroelastic torsional behavior of the flexible blade of a VAWT by considering the aerodynamic nonlinearities due to static stall and post-stall with the effects of a change in the Reynolds regime, the angle of attack, and the relative flow velocity due to the rotation of the turbine. Subsequently, the parameters considered in the developed method, namely the effects of stall, rotation, and Reynolds number on the torsion were evaluated. The results indicate that the presence of static stall reduces the amount of torsion. The angular velocity of the turbine creates an initial angle due to the effect of the centrifugal force in addition to changing the torsion curve, and applying the Reynolds regime of the flow leads to more accurate aerodynamic coefficients and results. Since the turbine undergoes large angles of attack while rotating (e.g. between +40° and -40° at TSR=1.5) and angles between +90° and -90° while stationary, linear aeroelastic computations produce erroneous results, and it is necessary to employ nonlinear aerodynamics while considering stall. A nonlinear aerodynamics model that can cover the whole range of angles of attack is essential. Hence, the difference in using linear aerodynamics, single-criterion nonlinear static stall aerodynamics, and multi-criteria nonlinear static stall aerodynamics in predicting the torsional behavior of the blade was subsequently evaluated. As expected, single-criterion nonlinear aerodynamics predicts a lower value for torsion at large angles than linear aerodynamics due to taking into account stall effects. However, at considerably larger angles single-criterion nonlinear aerodynamics is not capable of calculating the lift force due to not taking into account post-stall effects. These post-stall conditions were covered by adding extra second-degree polynomials. Then, by employing this complemented method, the aeroelastic torsion of the stationary turbine blade was evaluated at all possible blade positions at various wind velocities. As a result, Regions 2 and 7 (-90° to -45° and 45° to 90°, respectively) were determined to be the worst positions for parking the turbine in terms of critical torsion. Subsequently, the torsional behavior of the blade during one full rotation around the turbine at various TSR values was assessed by adding an angular velocity for the turbine. The corresponding results show that the blade undergoes aeroelastic torsion in the +7° to 12° range at higher TSR values and in the -4° to +19° range at lower TSR values. Thus, it is expected that operating the blade at high TSR values can prolong its lifespan.

Author Contributions

All authors planned the scheme, initiated the project, developed the mathematical modeling and examined the theory validation. The manuscript was written through the contribution of all authors. All authors discussed the results, reviewed, and approved the final version of the manuscript.

Conflict of Interest

The authors declared no potential conflicts of interest with respect to the research, authorship and publication of this article.

Funding

The authors received no financial support for the research, authorship and publication of this article.

References

[1] C. Jauch, J. Matevosyan, T. Ackermann, and S. Bolik, International comparison of requirements for connection of wind turbines to power systems, *Wind Energy*, 8(3), 2005, 295–306.
[2] K. Pope, G. F. Naterer, I. Dincer, and E. Tsang, Power correlation for vertical axis wind turbines with varying geometries, *Int. J. Energy Res.*, 35(5), 2011, 423–435.
[3] J. Lin, Y.-L. Xu, Y. Xia, and C. Li, Structural Analysis of Large-Scale Vertical-Axis Wind Turbines, Part I: Wind Load Simulation, *Energies*, 12(13), 2019, 1-31.
[4] Y. Li, *Straight-Bladed Vertical Axis Wind Turbines: History, Performance, and Applications*, IntechOpen, 2019.
[5] M. Islam, D. Ting, and A. Fartaj, Aerodynamic models for Darrieus-type straight-bladed vertical axis wind turbines, *Renew. Sustain. Energy Rev.*, 12(4), 2008, 1087–1109.
[6] N. Hettiarachchi, Overview of the Vertical Axis Wind Turbines, *Int. J. Sci. Res. Innov. Technol.*, 4(8), 2017, 56-67.
[7] J. Liu, H. Lin, and J. Zhang, Review on the technical perspectives and commercial viability of vertical axis wind turbines, *Ocean Eng.*, 182, 2019, 608–626.
[8] T. J. Carrigan, B. H. Dennis, Z. X. Han, and B. P. Wang, Aerodynamic shape optimization of a verticalaxis wind turbine using differential evolution, *Wind Turbine Technol. Princ. Des.*, 2011, Article ID 528418, 16p.
[9] L. Battisti, A. Brighenti, E. Benini, and M. R. Castelli, Analysis of different blade architectures on small VAWT performance, *J. Phys. Conf. Series*, 753(6), 2016, 62009.
[10] A. Meana-Fernández, L. Diaz-Artos, J. M. Fernández Oro, and S. Velarde-Suárez, Proposal of an Optimized Airfoil Geometry for Vertical-Axis Wind Turbine Applications, *Multidisciplinary Digital Publishing Institute Proceedings*, 2(23), 2018, 1464.
[11] I. Paraschivoiu, S. Shams, and N. V Dy, Performance assessment of Darrieus wind turbines with symmetric and

cambered airfoils, *Trans. Can. Soc. Mech. Eng.*, 42(4), 2018, 382–392.
[12] R. J. Templin, Aerodynamic performance theory for the NRC vertical-axis wind turbine, *NASA STI/RECON Tech. Rep.*, 76, 1974, 16p.
[13] J. H. Strickland, *Darrieus turbine: a performance prediction model using multiple streamtubes*, United States: N. P., 1975.
[14] I. Paraschivoiu, Double-multiple streamtube model for studying vertical-axis wind turbines, *J. Propuls. power*, 4(4), 1988, 370–377.
[15] I. Paraschivoiu, *Wind Turbine Design: With Emphasis on Darrieus Concept*. Polytechnic International Press, 2002.
[16] J. Katz and A. Plotkin, *Low-speed Aerodynamics*, Cambridge University Press, UK, 2001.
[17] D. Badiei, M. H. Sadr, and S. Shams, Nonlinear aeroelastic behavior of slender wings considering a static stall model based on wagner function, *Appl. Mech. Mater.*, 186, 2012, 297–304.
[18] R. Lanzafame and M. Messina, Advanced brake state model and aerodynamic post-stall model for horizontal axis wind turbines, *Renew. Energy*, 50, 2013, 415–420.
[19] M. S. Hameed and S. K. Afaq, Design and analysis of a straight bladed vertical axis wind turbine blade using analytical and numerical techniques, *Ocean Eng.*, 57, 2013, 248–255.
[20] S. Brusca, R. Lanzafame, and M. Messina, Design of a vertical-axis wind turbine: how the aspect ratio affects the turbine's performance, *Int. J. Energy Environ. Eng.*, 5(4), 2014, 333–340.
[21] W. Tjiu, T. Marnoto, S. Mat, M. H. Ruslan, and K. Sopian, Darrieus vertical axis wind turbine for power generation I: Assessment of Darrieus VAWT configurations, *Renew. Energy*, 75, 2019, 50-67.
[22] W. Liu and Q. Xiao, Investigation on Darrieus type straight blade vertical axis wind turbine with flexible blade, *Ocean Eng.*, 110, 2015, 339–356.
[23] T. Brahimi, F. Saeed, and I. Paraschivoiu, Aerodynamic Models for the Analysis of Vertical Axis Wind Turbines (VAWTs), *Int. J. Mech. Aerospace, Ind. Mechatron. Manuf. Eng.*, 10(1), 2016, 203-209.
[24] S. Shams, M. Kazemi, B. Mirzavand Brojeni, and Z. Khojasteh_Bakhteh Koupaei, Investigation of nonlinear aeroelastic behavior of airfoils with flow separation based on cubic static stall modeling, *Modares Mech. Eng.*, 16(12), 2016, 311–322.
[25] D. Marten, G. Pechlivanoglou, C. Navid Nayeri, and C. Oliver Paschereit, Nonlinear Lifting Line Theory Applied to Vertical Axis Wind Turbines: Development of a Practical Design Tool, *J. Fluids Eng.*, 140(2), 2017, 021107.
[26] Q. Li, T. Maeda, Y. Kamada, Y. Hiromori, A. Nakai, and T. Kasuya, Study on stall behavior of a straight-bladed vertical axis wind turbine with numerical and experimental investigations, *J. Wind Eng. Ind. Aerodyn.*, 164, 2017, 1-12.
[27] Z. Zhao *et al.*, Variable Pitch Approach for Performance Improving of Straight-Bladed VAWT at Rated Tip Speed Ratio, *Appl. Sci.*, 8(6), 2018, 957.
[28] J. Lin, Y. Xu, and Y. Xia, Structural Analysis of Large-Scale Vertical Axis Wind Turbines Part II: Fatigue and Ultimate Strength Analyses, *Energies*, 12(13), 2019, 2584.
[29] Z. Wu, G. Bangga, and Y. Cao, Effects of lateral wind gusts on vertical axis wind turbines, *Energy*, 167, 2019, 1212-1223.
[30] S. Shams and R. Esbati Lavasani, Derivation and Aeroelastic Analysis of a Rotating Airfoil Using Unsteady Loewy Aerodynamic and Flutter Suppression by PID Controller, *Modares Mech. Eng.*, 19(6), 2019, 1347–1354.
[31] R. E. Wilson and L. P.B.S., Machines power wind of aerodynamics, *Ntis Pb 238594*, no. Oregon State University, 1974.
[32] I. Paraschivoiu, Double-multiple streamtube model for Darrieus in turbines, In *NASA. Lewis Research Center Wind Turbine Dyn.*, 1981, 19-25.
[33] R. Sheldehl and P. Klimas, Aerodynamic Characteristics of Seven Airfoil Sections through 180-Degree Angle of Attack, *Report SAND80–2114. Sandia National Laboratories; Alberquerque*, New Mexico, USA, 1981.
[34] D. H. Hodges and G. A. Pierce, *Introduction to Structural Dynamics and Aeroelasticity,* Cambridge Aerospace Series, Vol. 15, 2011.
[35] E. H. Dowell, *A Modern Course in Aeroelasticity*, Springer International Publishing, 2015.

ORCID iD

Sh. Shams https://orcid.org/0000-0002-1259-821X
A. Molaei https://orcid.org/0000-0002-7793-0754
B. Mirzavand https://orcid.org/0000-0002-5666-5445